2026 NDIA MICHIGAN CHAPTER
GROUND VEHICLE SYSTEMS ENGINEERING
AND TECHNOLOGY SYMPOSIUM
POWER & MOBILITY TECHNICAL SESSION
AUGUST 11-13, 2026 - NOVI, MICHIGAN

INITIAL THERMAL EVALUATION OF 422 MARTENSITIC STAINLESS STEEL PISTON IN A HIGH-OUTPUT DIESEL ENGINE

Eric Gingrich[1], PhD[1], Michael Tess, PhD[1], Arkady Grunin[1], Vamshi Korivi, PhD[1], Katherine Sebeck, PhD[1], Dean Pierce, PhD [2], Yiyu Wang, PhD [2], Govindarajan Muralidharan, PhD [2], Rishi Pillai PhD [2], James A. Haynes, PhD [2], Kurt Will [3]

[1]US Army DEVCOM GVSC
[2]Oak Ridge National Laboratory
[3]Tenneco Powertrain

ABSTRACT

A piston manufactured with a crown comprised of grade 422 martensitic stainless steel and skirt manufactured from 4140 steel was instrumented with fifteen thermocouples and a wireless telemetry system. Piston temperature data were collected at five engine operating conditions and compared to two additional instrumented pistons with crown and skirt both made of 4140 martensitic steel, which is traditionally used for heavy-duty diesel applications. Thermal finite element modeling was used to predict the increase in operating temperature of the 422 piston relative to the 4140 piston and help understand instrumentation uncertainty. Previous research of candidate high-temperature alloys indicated that 12Cr martensitic steel alloys, such as alloy 422, offer several potential benefits when used in a diesel piston application, including increased high-temperature oxidation resistance and strength. The potential benefits of alloy 422 may however be partially negated by the expected increased piston operating temperature due to the alloy's lower thermal conductivity. In this work 422 alloy resulted in no statistically significant change in piston temperatures relative to the baseline 4140 steel during engine testing. The 422 alloy is poised to offer a dual durability advantage because the initial results show it can achieve superior oxidation resistance without operating at the higher temperatures that would accelerate such degradation. Maximum piston temperature capability is expected to be a critical design limit in next generation diesel engines with greater power density, lower heat rejection, and improved fuel economy.

Citation: E. Gingrich, et. al., "Initial Thermal Evaluation of 422 Martensitic Stainless Steel Piston in a High-output Diesel Engine," In *Proceedings of the Ground Vehicle Systems Engineering and Technology Symposium* (GVSETS), NDIA, Novi, MI, Aug. 11-13, 2026.

DISTRIBUTION STATEMENT A. Approved for public release; distribution is unlimited. OPSEC10780

1. INTRODUCTION

Heavy-duty (HD) diesel engines are likely to continue to be the primary power source for commercial on-road trucks for various reasons. While a high level of powertrain electrification is expected in the passenger car market, a transition to full battery electrification is not currently practical for commercial transport due to a number of technical limitations, including battery weight, size and recharge time [1] [2]. Similarly, military ground vehicles are likely to continue using diesel engines fueled by liquid hydrocarbons [3] for the foreseeable future. The high energy density and specific energy of hydrocarbon fuels make their storage, distribution and on-vehicle use advantageous throughout the spectrum of military operations, but particularly in austere or contested environments. These considerations motivate the continued research and development of more efficient, higher power density diesel engine powertrains for both the military and commercial transport sectors.

Diesel engine product offerings for commercial and military vehicles have diverged in the past decades, primarily because of the addition of emissions control equipment to meet regulatory requirements in commercial vehicles. U.S. military vehicles with armor, the engines on the other hand, are exempt from both the emissions certification requirements and fuel economy standards [4]. Regardless of this exemption, there is continual motivation for more fuel-efficient engines for military vehicles to increase range and reduce logistical demands related to fueling. Despite the diverging engine emissions standards, military powertrains have benefited from a number of advanced technologies developed for commercial use, including high-pressure common-rail fuel systems and improved single-piece steel piston designs that enable higher power density and longer service life. Historical and future trends suggest that advanced HD diesel engines will operate at higher peak cylinder pressures (> 250 bar) and temperatures to improve fuel economy and specific power output [5] [6]. The inherent linkage between cylinder pressure and heat transfer [7] [8] may cause piston temperatures to increase beyond the limits of the traditional steel piston alloys. Similarly, the pistons used in future military ground vehicle engines are likely to operate at increased temperatures because of the need for a compact, high-output propulsion system, which drives the typical military vehicle requirement for an engine that produces a large amount of power with the lowest possible heat rejection to the cooling system [9] [10]. Furthermore, U.S. Army vehicles are required to meet their mobility performance requirements in a range of environments, from sub-zero arctic (-40 °C) to extreme desert conditions (52 °C). The full load mobility requirements are particularly challenging to achieve at the hot ambient conditions due to engine cooling system limitations, thus exacerbating the piston thermal management problem. Consequently, the high temperature and pressure capabilities of steel piston materials are an area where commercial and military engine research efforts are aligned.

Medium carbon microalloyed steel 38MnSiVS5 (MAS) and quenched and tempered 4140 martensitic steel (4140) are the two primary alloys currently used in steel piston applications. The maximum operating temperature for these alloys depends on the specific engine and its service interval between major overhaul, but is typically restricted to a value between 500 to 550 °C because of strength and oxidation limitations [6]. Modern steel pistons typically feature a single-piece design manufactured by joining a bottom section, consisting of the skirt and wrist pin structure, to the piston crown [11] [12]. The geometry of the top and bottom sections is such that they form an annular oil cooling gallery (*i.e.,* "cocktail shaker" volume) when joined together through a weld process. A piston cooling nozzle (PCN) on the engine block aligns with and partially fills the gallery with engine oil when the piston is near bottom dead center (BDC). As the piston moves away from BDC, the continuous flow from the PCN impinges less in the gallery and splashes more on the volume enclosed by the under-crown region of the piston, connecting rod, and liner. The complex fluid-solid interaction in the cooling gallery has been studied [13] [14], but many analyses, including this one, are based on empirical calibration of the piston heat transfer coefficients by matching the thermal model predictions to measurements of steady-state piston temperature [15].

It is helpful to understand in-cylinder heat transfer in terms of the thermal pathway. The overall heat transfer starts with the high-temperature and high-pressure combustion products that transfer heat into the combustion chamber surfaces (which includes the piston) through convection. Although some radiation exists, the relative contribution is thought to be small compared to convective heat transfer [16], and radiation is often neglected in a simplified analysis of piston heat transfer. The heat is then conducted through the piston crown, which is typically less than 10 mm thick. On the bottom side of the piston facing the crankcase, the heat is transferred to the oil in the cooling gallery and to the other surfaces splashed on by the oil forming the under-crown region of the piston. This entire sequence can be simulated as a steady-state process (for a constant sustained engine load and speed), but in reality, the entire engine cycle is a transient process. Other heat sources such as piston ring and wrist pin friction exist, but many times are neglected because the majority of the heat flow is through the cooling gallery in modern steel pistons. The maximum piston temperature is sensitive to several parameters, including the heat flux input, the convection cooling from oil, the temperature dependent thermal conductivity of the piston material, and the wall thickness of a given material. All of these must also be considered when selecting a suitable piston alloy for a specific engine design.

Prior work by the authors focused on investigating the suitability of several martensitic steel grades for their potential suitability for HD piston applications [17] [18]. Utilizing engine modeling tools, material properties, and a coupon-level evaluation of cyclical oxidation in simulated combustion atmospheres, the study found that martensitic stainless steels with 12 wt.% chromium (12Cr) offered a good balance of strength, thermal performance, and oxidation resistance. Additional work has shown that alloys with Cr as low as 1 wt.% with 2 wt.% copper may provide a different pathway to achieve the balance of properties desired for HD pistons [19]. Furthermore, martensitic stainless steels with nominally 12 wt.% Cr and ~3 wt.% Cu are also under investigation for their remarkable oxidation resistance [20].

Martensitic stainless steels are used in a variety of high-strength and high-temperature applications such as stationary power generation (e.g., turbine blades), heat exchangers and pumps. The costs of martensitic steels are expected to be approximately two to five times the cost of 4140 in volume production. While the material costs are only a portion of the total piston cost, a martensitic stainless steel crown may increase welding, machining, and heat treating costs. Overall, the increase in cost of a finished piston with 422 crown and 4140 skirt is estimated to be 10-30% greater than a piston comprised only of 4140 steel. These costs are significantly less than Ni-based superalloys, where the raw material costs can be greater than fifty times the cost of 4140.

422 martensitic stainless steel, which is the subject of the current investigation, was one of the most promising steels previously studied [17]. The thermal and mechanical properties of martensitic stainless steel, 422 were further evaluated for suitability as a drop-in replacement for 4140 steel in HD pistons [18]. In cyclic oxidation testing, 422 was found to produce a protective chromium oxide layer up to 700 °C at 1000 h of testing in an atmosphere of air plus 10% water vapor. 650-700 °C is approximately the alloy's maximum operating temperature range in the piston application. The protectiveness of this oxide layer in 422 is however remarkably sensitive to heat variations in the Cr content of 422. For instance, in prior work [17] [20], a heat of 422 containing 12 wt.% Cr exhibited significantly better oxidation performance in lab scale cyclic oxidation testing at 700 °C in air and 10% and 30% water vapor contents compared to a heat containing 11.3 wt.% Cr. The chromium, among other alloying elements in 422, allows increased operating temperatures compared to 4140 but also substantially reduces the alloy's thermal conductivity by 20-45% over the temperature operating range 50-700 °C. Modeling and simulation tools indicated that the lower thermal conductivity would drive up piston temperatures and thus partially offset any improved oxidation performance at maximum temperature operating conditions. The inherent tradeoff of thermal conductivity and oxidation resistance motivates the current study to more rigorously investigate the piston operating temperatures of 422 and 4140 materials.

2. Experimental setup

Single-cylinder research engine (SCRE) experiments and complementary thermal finite element simulations were used to study the differences in piston temperature for pistons made with alloy 4140 and 422. Descriptions of each experimental tool are described next along with an assessment of the combined uncertainty of piston temperature.

2.1. Single-cylinder Engine Laboratory

Engine experiments were conducted on a single-cylinder research engine designed for high-output diesel operation. Full details of the engine laboratory and a similar wireless telemetry system can be found in Gingrich et al. [21]. A brief summary of the engine is provided here with engine specifications given in Table 1. Temperature-controlled combustion air, fuel, oil and coolant were provided to the engine from external systems that measured the mass flow rate of each fluid. The oil flow rate to a single PCN was also measured and controlled through an inline needle valve. PCN oil temperature was measured on the fluid stream before entering the nozzle. A high-pressure common rail system delivered fuel pressurized up to 2000 bar to a Bosch CRIN3 injector with an 8×167 μm hydro-ground nozzle (147° included angle).

All experiments were run using F-24, which is kerosene based jet fuel. The U.S. Army attempts to design and operate as many fuel-consuming devices with kerosene type fuels to reduce battlefield logistics [22]. For ground systems, this often means that engines designed to run on diesel fuel are operated using jet fuel. Overall, F-24 that meets the military fuel specifications, the ignition and combustion process is similar between diesel and jet fuels.

Table 1. Single-cylinder research engine specifications

Bore x stroke (mm)	122 x 128
Connecting rod length (mm)	239
Displacement (L)	1.496
Compression ratio (-)	14:1
Swirl ratio (-)	1.3
Piston crown wall thickness (mm)	6.4
Intake valve closing (°aTDC)	-108
Exhaust valve opening (°aTDC)	108

2.2. Thermocouple Instrumented Pistons

Three thermocouple-instrumented pistons, two with alloy 4140 crowns, and one with alloy 422 crown were used to acquire steady-state piston temperatures. Each piston was constructed in a two-piece design by joining the crown to skirt through a rotary friction weld process. All pistons, including 422 crown pistons, used a 4140 bottom forging for the skirt material, making it a multi-material piston. The 422 crowns were produced from the heat containing 12 wt.% Cr (designated 422C) in prior work [17] [20] see Table A.1 in the Appendix for full material composition. Producing quality welds utilizing a rotary friction weld process for multi-material pistons was challenging and was the subject of multiple investigations [23] [24] [25]. The mismatch of material strength, flow stress, carbon activity, carbon content and other material properties produced a non-symmetric weld interface and layered microstructure that needed refinement before pistons could be manufactured. Hereafter the nomenclature of 422 will be used to describe the multi-material 422/4140 piston and 4140-1 and 4140-2 for the two 4140/4140 pistons tested. All three telemetry pistons were instrumented in the same 15 locations across the piston crown. J-type, unsheathed thermocouples were installed nominally 1 mm below the combustion surface. Because the installation of the thermocouple involves drilling a blind hole, the exact junction location is unknown, but the axial placement uncertainty is expected to be less than ±0.5 mm. Figure 1b shows the projected thermocouple locations on the piston crown relative to other salient engine features; the bulk swirl direction is clockwise in this top-down view of the combustion chamber. Figure 1a shows the location of thirteen of the thermocouples installed in a plane perpendicular to the wrist piston axis, referred hereafter as the primary thermocouple axis. Thermocouples groups 1-6 and 10-15 are symmetric about the piston centerline, with thermocouple 8 (TC8) at the center of the piston. The primary thermocouple axis aligns closely with the injector spray plume axis. Figure A.1 in the Appendix show spray targeting.

Two additional thermocouples (TC), both at the same radial position corresponding to the bowl rim, were again installed in the crown 1 mm subsurface. TC 9 is installed in the crown located near the PCN inlet hole and TC 7 in the crown near oil drainage hole. These two thermocouples are on a plane bisecting the gallery holes for cooling oil supply and drainage, or an azimuthal angle 32.5° clockwise relative to the plane of the other 13 thermocouples. Overall, the design is similar to previous work [26] [17].

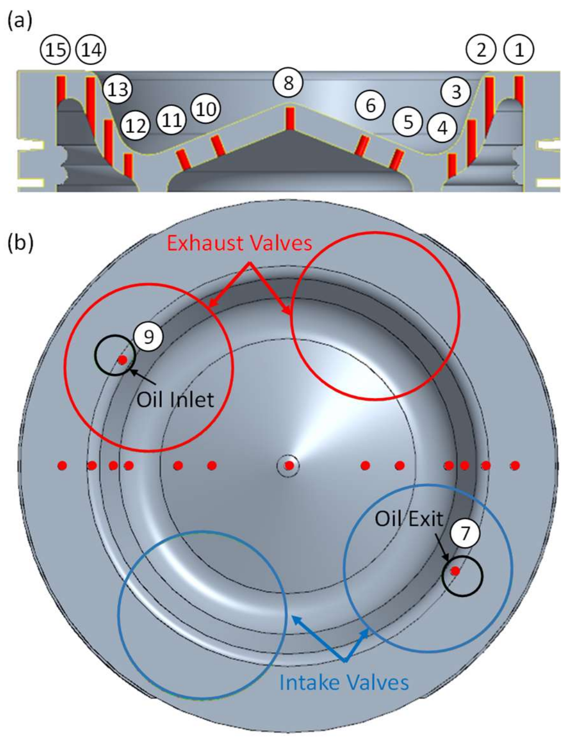

Figure 1: (a) Cross-section of thermocouple instrumented piston along primary axis (plane perpendicular to the wrist piston). Thermocouples are shown in red and numbered. (b) Top view of the thermocouple instrumented piston with superimposed thermocouple (red dots), piston cooling nozzle inlet, oil exit, exhaust valves and intake valves.

2.3. Test Matrix

Engine experiments are grouped into two sets: 1) baseline operating conditions and 2) sensitivity studies. For the baseline operating conditions, the engine was operated with a fixed speed and injection duration for each of the operating conditions shown in table 2. Operating conditions are similar to those used in prior work [21] [8] [27]. The load / speed selection was weighted toward high-load operation where piston temperatures are highest. Part-load, peak torque and rated power conditions typical of a production diesel engine were selected (conditions 1-3). Additionally, two very high output cases were included (conditions 4 and 5). Data were collected after all measured flows were allowed to stabilize. A start of injection (SOI) timing sweep was conducted for each of the operating conditions. When possible, data collection was randomized (operating conditions and SOI) to reduce progressively increasing errors. The crank-angle location of the 50% cumulative apparent heat release (CA50) is reported throughout this work rather than SOI. CA50 is an estimate of the 50% burn location. The injection duration was held constant, which meant load varied slightly with changes to SOI. For most cases the earliest injection timing was limited by the peak cylinder pressure limit of the SCRE, and the latest injection timing was limited by either exhaust temperature or exhaust smoke. The exhaust pressure target was set to a value slightly above or below the intake pressure, depending on condition.

Table 2. Operating conditions

Condition	Speed (r/min)	IMEPg (bar)	AFR(–)	Power Density (hp/L)
1	1700	11.23	30	14.4
2	1500	22.1	24	27.0
3	2500	19.3	26.9	33.0
4	1700	27.4	25	36.0
5	2750	27.4	26.6	52.3

A second set of experiments investigated the sensitivity of the measured temperatures to changes in select engine parameters. All sensitivity studies were conducted at operating condition 3. Table 3 shows the varied parameters and the range of values tested. Oil temperature, intake manifold temperature (IMT), PCN flow rate, and CA50 were investigated. Oil temperature and PCN flow rate studies were selected because they are thought to vary the amount of cooling on the under crown and oil gallery portions of the piston. Conversely, IMT and CA50 studies will impact the amount of heat transfer to the piston crown.

Table 3. Sensitivity studies at operating condition 3

Parameter	Values
Oil Temperature (°C)	70, 80, 90, 100
IMT (°C)	49, 67, 85, 103, 121
PCN Flow (kg/h)	440, 400, 350, 300, 250
CA50 (°ATDC)	-2.9, 1.4, 8.1, 11.0, 19.0

2.4. Simulation Setup

A finite element model was used to predict the temperature profile of the 4140 and 422 pistons at operating condition 5. The temperature-dependent thermal conductivity shown in Figure 2 was used in the model. It can be seen that the 422 thermal conductivity is substantially lower than 4140 across the temperature range. Based on prior work, a cycle-averaged heat flux input, calculated from a computational fluid dynamics (CFD) transient simulation that included moving valves & piston, turbulent flow, Lagrangian spray/evaporation and combustion, was assigned to the top surface of the piston bounding the combustion chamber [17]. On the piston oil gallery surfaces, cycle-averaged convective boundary conditions were assigned, calculated using a CFD/Volume of Fluid model that accounts for the motion of the piston and the oil flow within the piston cooling gallery [14]. Convective boundary conditions for the piston skirt and rings/groove were based on best practices from literature. Both the heat flux boundary conditions on the crown and the oil gallery / under crown region were steady state (time invariant) and spatially varying. The same boundary conditions were used for both 4140 and 422. The simplified boundary conditions are likely to result in overprediction of 422 crown temperature because the heat flux to the piston from the gas does not decrease as piston temperature increases.

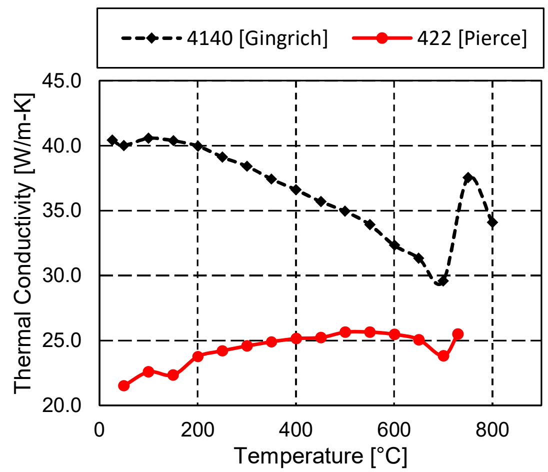

Figure 2: Thermal conductivity as a function of temperature for the investigated steels (4140 data are from [17] and 422 from [18]).

2.5. Uncertainty Analysis

Data sets are presented with error bars that represent the 95% confidence interval by combining accuracy and precision in quadrature. Each scalar value recorded by the data acquisition system represents a mean of 120 s of N data points that has a corresponding reported standard deviation, σ, which was used in: $t_{95:N-1}\sigma/\sqrt{N}$ to find the measurement precision, where $t_{95:N-1}$ is from the Student's t-distribution. The sensors' manufacturer specifications as a percent of reading, was used as the accuracy value in the combined total error. For fuel flow measurements, data from a system calibration (fuel cart including accessories) was used as a function of flow rate, which should represent a worse-case accuracy estimation for this device.

Piston temperature and temperature difference are presented using the same 95% confidence interval, but an investigation as part of the current work shows that this representation is likely a significant underestimation when comparing different instrumented pistons (see section 3.2).

3. Results and Discussion

This section describes the results for the simulation and experimental work comparing baseline alloy 4140 to 422. The simulation work describes the expected temperature change and is utilized to provide background on uncertainty of piston temperature measurements. The experimental results include five baseline conditions, sensitivity studies of targeted engine parameters, and global performance data.

3.1. Expected Temperature

A three-dimensional piston conduction model was used to compare the temperature difference between 422 and 4140 at operating condition 5. Figure 3 shows contours of the expected temperature increase on the crown of the high-temperature alloy relative to the baseline piston alloy. 422 shows a temperature increase of 24-104 °C. The largest increase on the bowl wall and lip is likely a result of these areas having the highest heat flux from the combustion chamber. The temperature increase of 422 compared to 4140 was expected given the lower thermal conductivity of 422 combined with the constant heat flux boundary condition on the crown of the piston and convective boundary condition on the backside. The relative increase of 422 is likely exaggerated because the crown heat flux boundary condition. The magnitude of temperature increase is significant compared to the maximum operating temperature of 422 which was previously shown to be in the range of 650-700 °C (100-150 °C increase from the 550 °C operating limit of 4140) in a cyclic oxidation rig [17]. As mentioned previously, the potential benefit of an increased maximum temperature limit may be partially offset by the increased operating temperature of 422. The temperature presented in figure 3 is subsurface to allow direct comparison to measured piston temperature. The temperature gradient between piston crown surface and thermocouple junction is on average 16 °C for 4140 and 23 °C for 422. The inherent simplification and uncertainty of simulated boundary conditions motivate the need for experimental measurements of piston temperature to evaluate the thermal performance of a 422 piston.

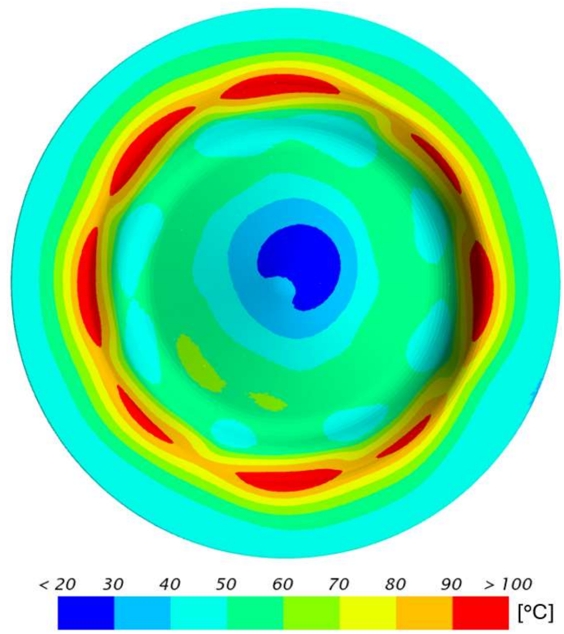

Figure 3: Simulation results for operating condition 5 showing the temperature difference (°C) between 422 and 4140, 1 mm subsurface

3.2. Prelude on Piston Temperatures

An introduction to piston temperature measurements and the associated uncertainty is needed to understand comparisons made in this work. This discussion is not intended to be an exhaustive list of uncertainties but rather provide a limited insight through experimental observation and analytical analysis. Throughout this paper, comparisons between 4140 and 422 are made under different conditions and the relative difference/change in temperature must be interpreted carefully with uncertainty in mind.

A subset of 4140 experiments were repeated using two different pistons instrumented with thermocouples which allows repeatability to be evaluated. Figure 4 shows piston temperature as a function of piston radius for 4140-1 and 4140-2. The thermocouples on the diameter perpendicular to the wrist piston (TC 1-6, 8, 10-15) are shown with markers connected by lines to the adjacent thermocouple. Thermocouples 7 and 9 are included on the plot at ±45 mm radius, but do not have connecting lines (see red arrows). The piston bowl profile is shown in orange on the right y-axis. Throughout this paper multiple piston temperatures are presented in the same manner as Figure 4. Thermocouple numbering in these figures is consistent with Figure 1 (numbered right-to-left).

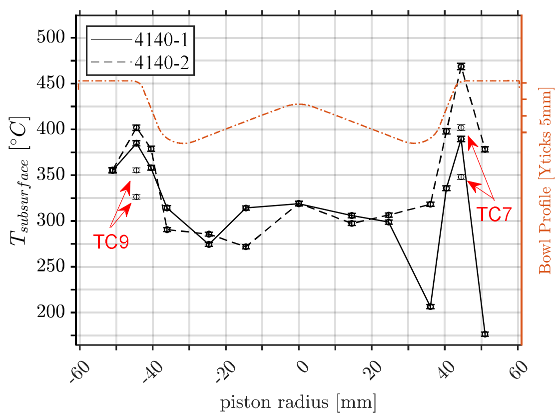

Figure 4: Operating condition 3, CA50=2°aTDC, subsurface piston temperature versus piston radial location for 4140-1 and 4140-2. The piston bowl profile is outlined by the dash-dot orange line (right y-axis).

Ideally, the measured temperatures of both 4140-1 and 4140-2 should lay on top of each other. However, a large discrepancy at thermocouples 1 (+51 mm) and 4 (+36 mm) is observed. The sensors at these two locations were investigated further after engine testing, and it is believed that the temperature was erroneous due to a short in the thermocouple wires which resulted a junction forming on the bottom side of the piston. On subsequent plots, data from these two sensors are removed from 4140-1.

Differences between 4140-1 and 4140-2 at other thermocouple locations range significantly from nearly 0 °C at the center to 75 °C at thermocouple 2 (+45 mm radius). The sources of these differences are not entirely clear, but it is thought to stem from variation in piston instrumentation. Thermocouples are drilled and installed from the bottom (skirt) side of the piston and have an associated machining tolerance which will impact the thermocouple junction location relative to the piston crown. The wire routing, epoxy, and metal straps part of the telemetry system installation may impact the overall resistance pathway for heat to be rejected to the oil.

To understand the potential impact of thermocouple installation variance, the piston thermal model used to predict temperature difference was also used to calculate the thermal gradient across the piston crown. Figure 5 shows predicted thermal gradients with overlayed thermocouple locations on the piston crown. The gradient presented is combined in quadrature from the x, y, and z directions. The values range from 15-40 °C/mm at the sensor locations with lower gradients for the locations closer to the center of the piston for condition 5.

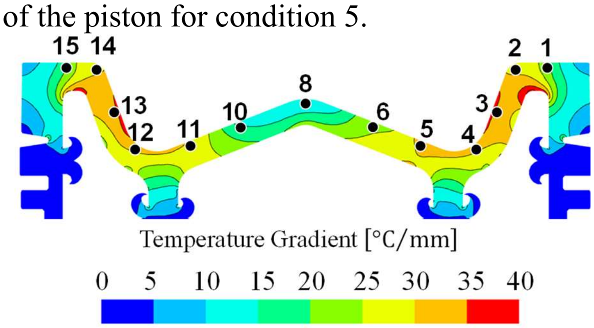

Figure 5: Predicted piston thermal gradients with overlayed thermocouple locations

If the variance of thermocouple location is ±0.5 mm, the contours can be used to estimate the difference in temperature from sensor location and is estimated at ±7.5-20 °C. Comparing these values to the observed difference between 4140-1 and 4140-2 at thermocouple 2 (+45 mm radius) in Figure 4, the total estimated temperature variance is less than the observation in the SCRE experiments. Therefore, it is reasoned that other uncontrolled sources of variation are likely present.

An additional source of instrumentation variation may stem from thermocouple wire routing. Wires are adhered to the back side of the piston through spot welded straps and epoxy which may impact piston oil cooling. Although effort is made to keep wire routing and attachment similar, variation was present and the resulting temperatures changes are difficult to quantify.

Engine build-to-build variance, engine wear, and other differences in the experimental setup, have minimal impact on temperature uncertainty. For all builds the same engine hardware (other than the piston) was used. Although not presented in this work, repeatability studies, including multiple installations of the PCN, were conducted to understand the impact to piston temperature data. The SCRE allows precise control of boundary conditions. Additionally, in-cylinder pressure measurement allows for confirmation that in-cylinder conditions are consistent across engine builds.

In this work, it was determined that each instrumented piston required 20-30 hours of engine operation before temperature measurements stabilized. An initial upward trend at some thermocouples locations bounded by oil gallery was observed. The root cause of the temperature increase is unknown, but could be related to surface effects in the oil gallery surfaces. Changes to the epoxy adhesion or chemical stability may impact oil heat transfer. Other surface effects such as a buildup of a thin, veneer-like layer would also cause an increase in thermal resistance and result in an increased temperature. The buildup of a carbon layer from oil coking is not thought to be a contributing factor because no dark-colored buildup was observed on the bottom of any of the telemetry pistons, and because the temperature increase stabilized after the initial run-in period.

When available, subsequent figures in this work include both 4140-1 and 4140-2 to emphasize that uncertainty/variability of the test data when compared to 422. The presentation of the piston temperature data as an averaged temperature in some figures is thought to limit bias and uncertainty that may be present from any individual sensor. Some figures also utilized temperature difference for parametric studies. Because the difference is calculated between two conditions using the same telemetry piston, individual sensor bias should be reduced compared to absolute temperature. Piston temperatures include error bars that combine precision and accuracy of the measurements (see experimental setup section) which is typically around ±3 °C. The authors recognize that these error bars are likely optimistic in comparison of 4140 to 422. This presentation choice was made because actual uncertainty is a subjective interpretation based on the previous factors and may vary for each sensor and operating condition.

3.3. Piston Temperature: Baseline Conditions 1-5

The SCRE was run over five load/speed combinations as listed in Table 2. For each operating condition, a start of injection (SOI) sweep was conducted which resulted in a range of combustion phasings, which are represented by the CA50 timing. When evaluating piston temperature, comparisons should be made at constant CA50 (or as close to constant as possible) because small changes to CA50 result in significant changes in piston temperature [26]. Changes in CA50 result in relatively large changes to in-cylinder pressure and bulk temperature which drives piston crown heat flux and subsequently piston temperature.

Figure 6 shows average piston temperature utilizing all 15 thermocouples for all five operating conditions across all CA50s tested. The average was calculated using a simple arithmetic mean (rather than assigning sensor weighting factors based on surface area). The simple mean is thought to reduce measurement uncertainty because the sensors that would have a larger area weighting factor may also have the largest uncertainty from difficulty of sensor drilling and wire routing. Each operating condition is represented by a unique marker style and color is used for material type: black for 4140 and red for 422. Operating conditions 2-5 shows 4140 10-25 °C hotter than 422 across the CA50s tested. Operating condition 1 has nearly matched average piston temperature across the CA50 range. The expected heat load on the piston is expected to be much less for condition 1 than other conditions because it is a part-load condition with lower in-cylinder pressure and bulk temperature.

The data in Figure 6 is not shown with error bars for visual clarity. Uncertainty combining precision and accuracy is around ±3 °C but does not include other bias that may impact measurements (see early discussion in section 3.2). Operating condition 1 temperature difference falls within the uncertainty of the measurements. Operating conditions 2-5 temperature difference between 4140 and 422 is a bit more difficult to evaluate with uncertainty in mind. Some of the operating conditions are within the uncertainty bounds and others show a temperature difference that may be significant.

Rather than attempting to arbitrate the significance of each condition and CA50 combination, the more important observation is that regardless of temperature differences between 4140 and 422, 4140 operates at a higher average temperature compared to 422. This was unexpected and contrary to the expected result. Recall that the simulated temperature difference of operating condition 5 shown in Figure 3 shows 422 to be 24-104 °C hotter than 4140 -this trend is clearly not present in the experimental data.

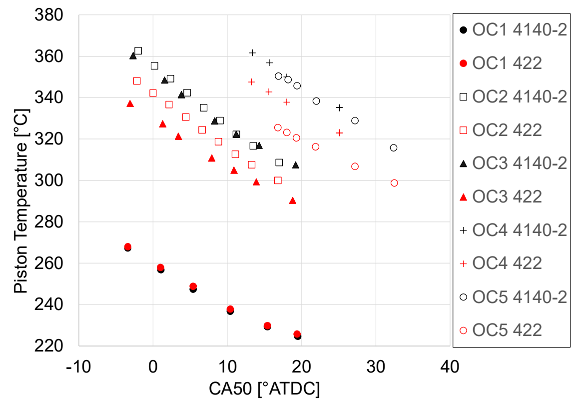

Figure 6: Operating conditions 1-5 average subsurface piston temperature versus CA50 location for 4140-2 and 422.

Subsurface piston temperature at each measurement location is shown in Figures 7 and 8 for operating conditions 1 (CA50=1°aTDC) and 3 (CA50=2°aTDC), respectively. Operating conditions 2, 4, and 5 were similar to operating condition 3, so they are included in the Appendix (see Figures A.2, A.3, and A.4, respectively). Only one CA50 is included because the temperature distribution across the piston is similar for each CA50 with average temperature increasing as CA50 is advanced (see Figure 6). Spatial changes in temperature will be discussed in Section 3.4 as part of the sensitivity studies.

The subsurface temperature in Figure 7 shows good agreement between 4140-1, 4140-2, and 422. 4140-2 and 422 have temperatures so similar at most locations that it is sometimes difficult to discern the markers and lines on the plot because they overlap. 4140-1 and 4140-2 are generally considered to have good agreement at most locations. An exception to this trend is at +40 and +45 mm locations, which shows a difference of 25 and 50 °C, respectively. These differences are thought to be because of variability in the physical piston instrumentation.

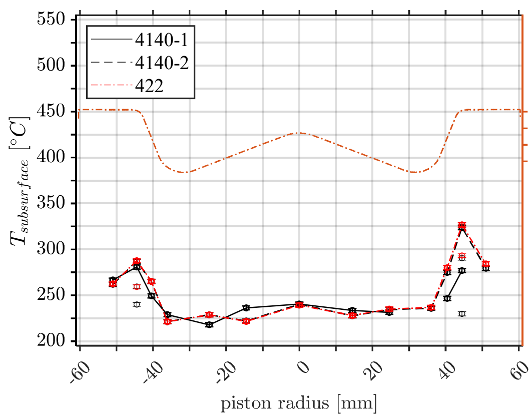

Figure 7: Operating condition 1, CA50=1°aTDC, subsurface piston temperature versus piston radial location for 4140-1, 4140-2, and 422. The piston bowl profile is outlined by the dash-dot orange line (right y-axis).

Figure 8 shows the subsurface temperature distribution as a function of radius for condition 3 (CA50=2°aTDC). The higher load of this condition compared to condition 1 results in high piston temperatures and relative differences in the temperature data are more apparent. The data for 4140-1 and 4140-2 are the same as Figure 4 but the outlier data are removed. 422 temperature data are now included in the plot. The thermocouples toward the center of the piston on the under crown region (between -27 mm +27 mm) shows 422 approximately 25-50 °C cooler than 4140. This difference can vary based on location and whether 4140-1 or 4140-2 is used as the baseline, but overall, there appears to be a trend in the under crown region of the piston. It is more difficult to identify other temperature trends comparing 422 to 4140. When comparing temperature along the primary axis (plot markers connected with lines), multiple cross over points between 4140 and 422 are observed. No other spatial trends at multiple adjacent thermocouples are visible. When comparing across the positive and negative radii of the piston, no obvious trends stand out. For example, the temperature at the ±51 mm location shows opposite trends: the -51 mm location shows 4140 about 75 °C hotter than 422, but at +51 mm 4140 is about 50 °C cooler.

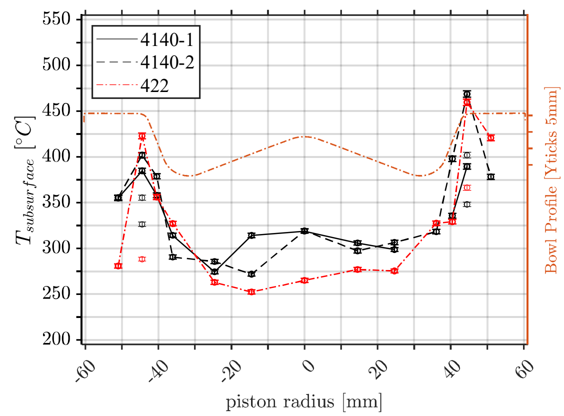

Figure 8: Operating condition 3, CA50=2°aTDC, subsurface piston temperature versus piston radial location for 4140-1, 4140-2, and 422. The piston bowl profile is outlined by the dash-dot orange line (right y-axis).

Comparing 422 to 4140 for the five operating conditions, the authors want to emphasize that the predicted temperature increase of 422 relative to 4140 was not realized in the single-cylinder test data. This is surprising. This finding may indicate that 422 could provide additional temperature capability because its oxidation limit is around 700 °C, which is well beyond the 500 °C limit for 4140. Further engine durability testing is needed to investigate this finding with higher certainty.

3.4. 422 Thermal Behavior

As to why the 422 behaves much different than expected, a few potential reasons can be hypothesized. As previously discussed in Section 3.2, measurement uncertainty related to instrumentation and thermocouple placement may account for no more than ±20 °C. When an average piston temperature is calculated as in Figure 6, any random error in thermocouple placement should, on average, be minimized, which should limit the error of the average temperature. The predicted temperature difference of the alloys for condition 5 shows 422 over 100 °C hotter in the piston bowl region, which should be detectable in the engine experiments given that this is a factor of 5 times larger than the instrumentation and thermocouple placement uncertainty. Because the average temperature of 422 is less than 4140 in the experiments, other physical explanations are needed beyond instrumentation uncertainty.

Possible explanations are given in the context that they impact piston heat transfer, which is a complex process which involves heat transfer from the hot combustion chamber gas, conduction though the piston wall, and convection to the cooling oil. In the combustion chamber, convection is thought to drive heat from the combustion gas to the piston crown and a smaller portion of heat is thought to be from radiation from the hot gas and particulates to the piston. Even though most combustion models neglect radiation because it is difficult to model, differences in 422 and 4140 material emissivity and the different type, thickness, and amounts of porosity in the surface oxides they form could impact radiation.

Although every effort was made to manufacture 4140 and 422 pistons as similar as possible, some observed differences may impact piston heat transfer. First, both pistons are coated with a Manganese Phosphate (MnP) coating for wrist pin lubrication [28]. The coating process is a dip process where all surfaces of the piston are coated including the crown and oil gallery. 422 piston crowns were masked off prior to coating so no coating is present on the 422 piston crown. Adhesion of the MnP coating on the 422 under crown and oil gallery region was spotty with some regions with no visible coating. Coating adhesion, microstructure, porosity, and thickness differences may impact the surface thermal resistance and may have an impact on heat transfer in the oil gallery.

Another consideration is differences in the piston crown wall thickness. For this work, machining and welding tolerances are estimated to account for variations in wall thickness on the order of ±0.2 mm. Changes in wall thickness will impact the conduction length where heat moves and may change the balance of temperature on the piston. Samples were selected with total similar weld upset (±0.05mm) which should result in similar crown wall thicknesses. Weld upset is the total reduction in the axial length of the workpieces (crown and skirt) that occurs as they are joined during the rotary friction welding process. This shortening happens because the intense heat and axial pressure cause the materials at the interface to plastically deform and flow outward, creating a characteristic flash around the joint

Additionally, the weld flash geometry formed during the rotary friction weld process is different for 422 and 4140 pistons. Figure 9 shows an overlay of a 4140 (green) and 422 (gray) pistons (figure 9a) and sectioned 422 piston (figure 9b). The blue dotted line on figure 9b denotes the weld interface and the curled in material is the weld flash. For 4140 piston the curled in material is mostly symmetric top-to-bottom where an asymmetry flash is formed for the 422 piston. Figure 9a shows that the weld interface for the 422 piston has moved down compared to the 4140 piston. The two materials that comprise the 422 piston have different strength and high-temperature forging properties which results in different weld flash geometry and differences in which side of the weld takes up weld upset. For geometry details see Wang et al. [23] [24] [25]. The difference between 422 and 4140 weld geometry is small compared to the size of the oil gallery so it is reasoned that oil flow, and consequently, heat transfer, in the gallery should be minimally impacted. Because engine heat transfer is complex further investigation is needed.

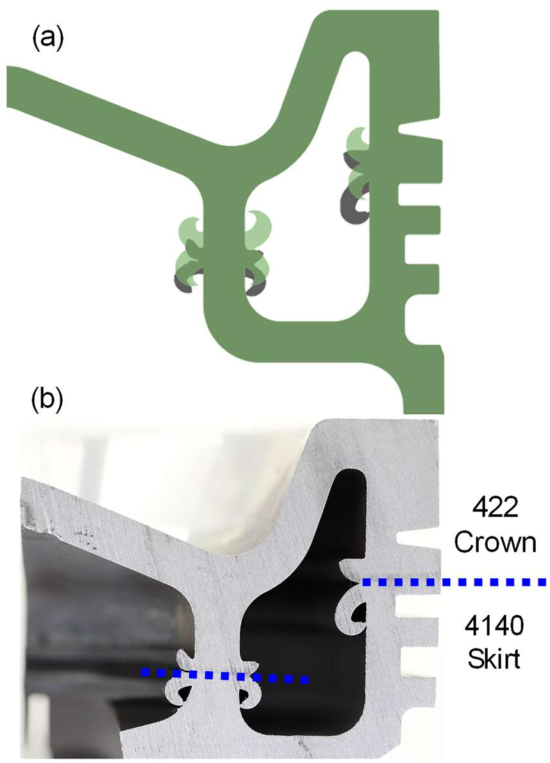

Figure 9: (a) Overlay of 4140 (green) and 422 (gray) piston sections (b) 422 piston cross-section with weld interface shown blue dotted line

The discrepancy between the predicted and experimental results suggests that the current model may not account for all physical phenomena. It is hypothesized that several factors, not included in the current analysis, could be contributing. Overall, all the geometry differences between 422 and 4140 pistons are considered small and authors don't believe that any single difference can be attributed to the current observations. Additional experimental and modeling work is needed to investigate the current results further. However, it is beyond the scope of this work to provide a definitive answer.

3.5. Piston Temperatures: Sensitivity Studies

Sensitivity studies of oil temperature, IMT, PCN flow rate, and CA50 were conducted to observe the piston temperature response for 422 and 4140. Each parametric study had between four and six values tested, and a self-imposed limit of 500 °C for the maximum piston temperature was followed for repeatability reasons. To present the large data set, two summary plots for each study were generated. First, the average (mean of all 15 TCs) and maximum temperature (at TC2) as a function of the parameter studied are presented in the Appendix in Figures A.5-A.8. A best fit line was added to the mean and maximum temperature data. The slope of the line is summarized in Table 4 with units. Over the range of parameters investigated, a line was considered a good fit with least squares residual, R, greater than 0.98 for all data sets except the PCN flow rate, which had values greater than 0.85. Figures 10-13 quantifies the spatial variability by calculating the difference between each extreme of the parametric study, and thus presents the temperature difference as a function of piston radius.

The sensitivities in Table 4 should only be compared to other values in the same sensitivity study because the units are different in each study. When comparing the 4140 column to the 422 column, as a general comment, the sensitivities are similar for both materials. The average (mean of all 15 TCs) and maximum (at TC2) are both tabulated. The average is thought to have a lower uncertainty, but the authors thought it was also important to report on the maximum temperature location (which always occurred at thermocouple 2 on the bowl lip in this work). For diesel engines operating near a piston temperature limit, understanding the sensitivity at the maximum temperature location may be more important than the average.

Table 4. Sensitivity of average and maximum (TC2) piston temperature to oil temperature, IMT, PCN flow, and CA50.

Parameter		4140	422
Oil Temperature	Mean	0.55	0.7
[°C Piston / °C Oil]	Max	0.46	0.56
IMT	Mean	0.35	0.31
[°C Piston / °C IMT]	Max	0.52	0.52
PCN Flow	Mean	-0.092	-0.091
[°C Piston / (kg/h)]	Max	-0.067	-0.052
CA50	Mean	-2.45	-2.17
[°C Piston / °aTDC]	Max	-3.06	-3.2

Figure 10 shows the change in piston temperature between CA50 of 2 and 20 °aTDC across the piston radius. As CA50 is advanced, both the in-cylinder pressure and bulk in-cylinder gas temperature increase and subsequently the heat flux from the combustion gas to the piston is increased [21]. The temperature increases for both 4140 and 422 are similar, with the piston bowl wall and rim (35 to 45 mm and -35 to -45 mm) showing the largest increase. As combustion phasing is advanced, more of the combustion event is likely occurring in the piston bowl, with more hot reacting fuel impinging on the bowl wall and rim.

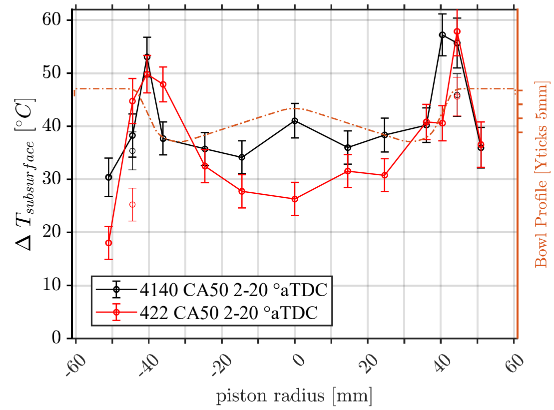

Figure 10: Operating condition 3 subsurface piston temperature difference between CA50=2°aTDC and CA50=20°aTDC for 4140-2 and 422. The piston bowl profile is outlined by the dash-dot orange line (right y-axis).

Figure 11 shows the change in piston temperature for the oil temperature sweep of 100 °C and 70 °C. Oil temperature values reported are based on the temperature measurement location at the oil feed to the PCN. The oil sprayed on the back side of the piston changes the amount of cooling on the underside of the piston. The response to changes in oil temperature for both 4140 and 422 are similar. Across the radius of the piston, the change in piston temperature is relatively flat compared to the sensitivity studies, of CA50, PCN flow, and IMT.

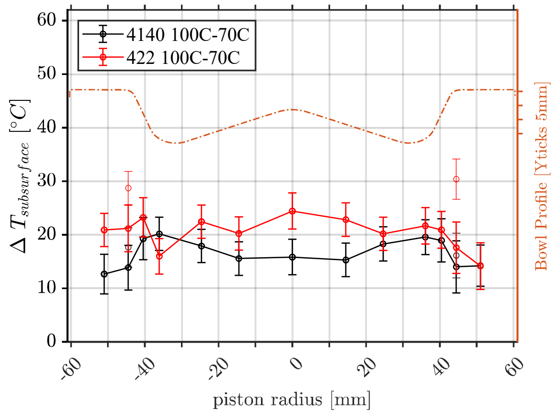

Figure 11: Operating condition 3, CA50=2°aTDC, subsurface piston temperature difference between oil temperature of 100°C and 70°C for 4140-2 and 422. The piston bowl profile is outlined by the dash-dot orange line (right y-axis).

The change in piston temperature between PCN flow rate of 250 and 440 kg/hr is reported in Figure 12. Recall that the location of PCN targeting on the underside of the piston is shown Figure 1. The oil inlet hole on the piston corresponds to -45 mm and is not part of the primary thermocouple axis, so temperature is represented with a marker on the plot not connected to other locations with a line. The responses of 4140 to 422 are similar with one notable exception at +25 mm: at this location, 422 temperature increases much faster than 4140 as PCN flow is decreased. It is not immediately clear why this discrepancy occurs. This location does not show a similar trend in other sensitivity studies so a thermocouple issue is not suspected. The piston under crown includes five thermocouples bounded in this ±25mm radius region, which includes the sensor with the largest discrepancy. The under crown region is not bounded by the oil gallery, and therefore cooling is achieved by indirect oil spray from the PCN, an oil drain passage at the top of the connecting rod (supplying lubrication to the wrist pin), as well as oil splash from inside the crankcase. Because of its indirect cooling, the under crown region may be more sensitive to changes in PCN flow than thermocouples bounded by the oil gallery which captures oil for a "cocktail shaker" effect [15]. Small differences in instrumentation hardware (see section 3.2) could impact indirect oil flow and result from variations in local sensitivity when comparing 4140 to 422.

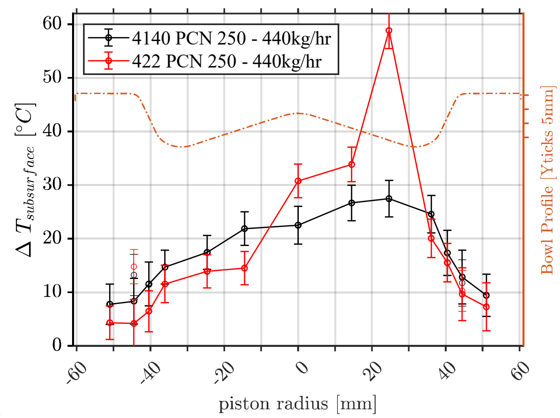

Figure 12: Operating condition 3, CA50=-3°aTDC, subsurface piston temperature difference between PCN flow of 250 kg/hr and 440kg/hr for 4140-2 and 422. The piston bowl profile is outlined by the dash-dot orange line (right y-axis).

Figure 13 shows the piston temperature difference as IMT is increased from 49 to 121 °C. Increasing the IMT increases the combustion gas temperature with nearly constant in-cylinder pressure. The increased gas temperature drives up the heat flux on to the piston and subsequently the piston temperature. The response of 4140 compared to 422 is similar across the piston radius.

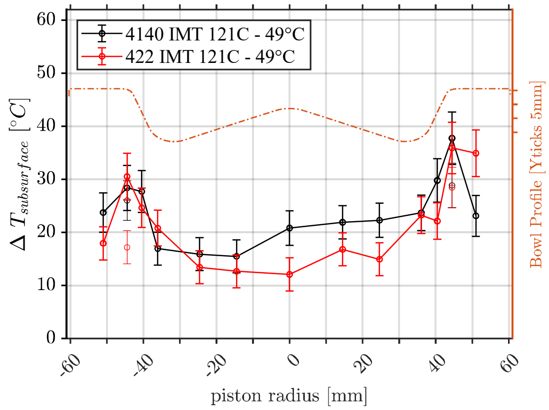

Figure 13: Operating condition 3, CA50=3.5°aTDC, subsurface piston temperature difference between intake manifold temperature of 121°C and 49°C for 4140-2 and 422. The piston bowl profile is outlined by the dash-dot orange line (right y-axis).

In summary, the temperature responses of 4140 and 422 were similar for the parametric studies of CA50, oil temperature, PCN flow rate, and IMT. Although some discrepancies exist at individual sensor locations, most locations show temperature differences that are judged to be insignificant.

3.6. Global Engine Performance

In addition to the piston temperature measurements, indicated engine performance data was acquired. In-cylinder pressure combined with other measurements were used to calculate gross indicated thermal efficiency (ITEg) and indicated specific heat rejection ($\dot{Q}_{gas}/\dot{W}_{i,g}$). To calculate indicated specific heat rejection, the heat transfer from the in-cylinder gas, $\dot{Q}_{gas}$, is calculated and normalized gross indicated power, $\dot{W}_{i,g}$; see [27] for additional details. Figure 14 shows the ITEg as a function of CA50. The optimal CA50 is slightly after top dead center for maximum efficiency. Over the CA50 range investigated, the data for both 4140 and 422 lie on top of each other without any significant difference. Similarly, Figure 15 shows indicated specific heat rejection as a function of CA50, and again does not show a difference between 4140 and 422 beyond the range of the error bars. The overall trend does however show 422 with a lower indicated specific heat rejection at nearly all CA50s which may be from a reduction in piston heat transfer.

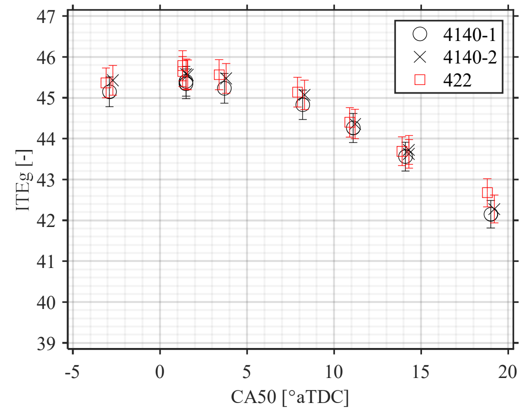

Figure 14: Operating condition 3 gross indicated thermal efficiency as a function of CA50 combustion phasing for 4140-2 and 422.

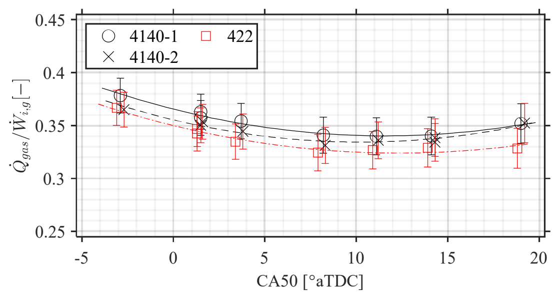

Figure 15: Operating condition 3 work specific heat rejection as a function of CA50 combustion phasing for 4140-2 and 422.

The ITEg and indicated specific heat rejection are examples of global performance data, but more broadly, other global measurements were also acquired on the SCRE and similarly did not show a meaningful difference when comparing 4140 to 422. The global measurements provide insight into how the fuel energy is distributed into useful work, heat transfer, exhaust enthalpy, or other losses. Another possible explanation for why the predicted temperature increase of 422 relative to 4140 was not realized in the experiments is that the heat transfer into the piston was reduced, which would in turn result in piston temperatures lower than predicted in Figure 3. None of the global data support this explanation given the results for 4140 and 422 are similar. Prior engine CFD simulations [17] and experimental work [29] showed a slight downward trend in the heat transfer for 422 under high load operating conditions, so the hypothesis that reduced engine heat transfer is impacting 422 piston temperature needs further investigation.

A visual inspection of the 422 piston was conducted after SCRE testing. No unusual oil coking or deposits were found on the under crown region of the piston. A picture of the piston crown combustion chamber surface is shown in Figure 16. A chromatic, rainbow-colored pattern observed was observed on the piston bowl. Prior work indicates that the growth of a thin, chromium-rich oxide surface layer may present in such a way and has been found to provide protection against deleterious oxidation up to around 700 °C [17] [18] [20]. The chromatic pattern is most visible between the dark spray impingement marks caused by fuel injection and combustion. Further analysis through piston sectioning and microscopy is needed to confirm oxide growth and type.

Figure 16: 422 piston, post engine test

4. CONCLUSIONS

Piston temperatures were acquired for pistons made of 422 stainless steel and 4140 steel crowns. Temperature data were collected at five engine operating conditions and at targeted parametric studies of intake temperature, piston cooling nozzle oil flow, and oil temperature, CA50.

- Contrary to initial expectations, 422 alloy resulted in no statistically significant change in piston temperatures relative to the baseline 4140 steel during engine testing. This result was initially regarded as counterintuitive, as the predicted temperatures of 422 were up to 104 °C hotter, driven by thermal conductivity of the 422 which is approximately 25% lower than that of 4140 steel at 550 °C.
- A contributing factor thought to partially explain the unexpected piston temperatures is measurement uncertainty arising from thermocouple placement and other variations in instrumentation. The simulation framework was therefore used to investigate this possibility by modeling the internal temperature gradients of the piston and quantifying their sensitivity at the precise measurement locations. The temperatures measured at these high-gradient areas of the piston are inherently

sensitive to positional variance, meaning that seemingly minor, as-manufactured deviations in thermocouple placement on the order of ± 0.5 mm could introduce a measurement bias of up to ± 20 °C.

- For each sensitivity study, 4140 and 422 had a similar piston temperature response to parametric changes to intake temperature, piston cooling nozzle oil flow, oil temperature and CA50. Similarly, SCRE thermal efficiency, specific heat rejection, and other global performance metrics were found to be comparable for both 422 and baseline 4140 experiments.
- A visual inspection of the 422 piston after testing showed no unusual oil coking or deposits. A chromatic, rainbow-colored pattern observed on the piston surface indicates potential growth of a thin, chromium-rich oxide surface layer which has been found in prior work to provide protection against deleterious oxidation up to 700 °C.
- The 422 alloy is poised to offer a dual durability advantage because the initial results show it can achieve superior oxidation resistance without operating at the higher temperatures that would accelerate such degradation. Additional testing at extreme piston temperature conditions and longer operating time is needed to assess the potential benefits of alloy 422.

5. REFERENCES

[1] G. Kalghatgi, "Is it really the end of internal combustion engines and petroleum in transport?," *Applied energy,* vol. 225, pp. 965-974, 2018.

[2] S. Sripad and V. Viswanathan, "Performance metrics required of next-generation batteries to make a practical electric semi truck," *ACS Energy Letters,* vol. 2, no. 7, 2017.

[3] The National Academies of Science, Powering the U.S. Army of the Future, 2021.

[4] P. Schihl, "On the Availability of Commercial Off-the-Shelf (COTS) Heavy-Duty Diesel Engines for Military Ground Vehicle Use," *SAE International Journal of Engines,* vol. 2, pp. 1520-1527, 2009.

[5] Z. Mills, C. Finney, A. Haynes, A. Trofimov, H. Wang and D. Pierce, "Impact of Materials Properties on Higher-Temperature Engine Operation," *SAE International Journal of Advances and Current Practices in Mobility,* vol. 4, pp. 448-461, 2021.

[6] D. Pierce, A. Haynes, J. Hughes, R. Graves, P. Maziasz, G. Muralidharan, A. Shyam, B. Wang, R. England and C. Daniel, "High temperature materials for heavy duty diesel engines: Historical and future trends," *Progress in Materials Science,* vol. 103, pp. 109-179, 2019.

[7] G. Woschni, "A Universally Applicable Equation for the Instantaneous Heat Transfer Coefficient in the Internal Combustion Engine," *SAE Technical paper,* 1967.

[8] E. Gingrich, M. Tess, V. Korivi and J. Ghandhi, "High-output diesel engine heat transfer: part 2--instantaneous spatially averaged heat transfer correlation," *International Journal of Engine Research,* vol. 23, pp. 1435-1452, 2022.

[9] Southwest Research Institute, "Research Need for More Compact Intermittent Combustion Propulsion

Systems for Army Combat Vehicles-Volume I," 1995.

[10] Southwest Research Institute, "Research Need for More Compact Intermittent Combustion Propulsion Systems for Army Combat Vehicles-Volume II," 1995.

[11] P. Kemnitz, O. Maier and R. Klein, "Monotherm, a New Forged Steel Piston Design for Highly Loaded Diesel Engines," in *SAE 2000 World Congress*, 2000.

[12] M. Maurizi and D. Hrdina, "New MAHLE Steel Piston and Pin Coating System for Reduced TCO of CV Engines," 2017.

[13] J. Lahr, "Experimental and Computational Analysis of Oil Flow in Cooling Galleries of Diesel Engine Pistons," PhD Dissertation, Birmingham City University, 2016.

[14] A. Grunin and V. Korivi, "Oil flow and heat transfer for gallery-cooled pistons," in *In Proceedings of the Ground Vehicle Systems Engineering and Technology Symposium (GVSETS)*, Novi, MI, 2023.

[15] J. Pan, R. Nigro and E. Matsuo, "3-D Modeling of Heat Transfer in Diesel Engine Piston Cooling Galleries," in *SAE 2005 World Congress*, 2005.

[16] J. Benajes, J. Martin, A. Garcia, D. Villalta, A. Warey, V. Domenech and A. Vassallo, "An investigation of radiation heat transfer in a light-duty diesel engine," *SAE International Journal of Engines,* vol. 8, pp. 2199-2212, 2015.

[17] E. Gingrich, D. Pierce, G. Byrd, K. Sebeck, V. Korivi, G. Muralidharan, H. Wang, J. Torres, A. Trofimov, J. Haynes and M. Tess, "Evaluation of high-temperature martensitic steels for heavy-duty diesel piston applications," *SAE International Journal of Advances and Current Practices in Mobility,* vol. 5, 2022.

[18] D. Pierce, G. Muralidharan, A. Trofimov, J. Torres, H. Wang, J. Haynes, K. Sebeck, E. Gingrich, G. Byrd and M. Tess, "Evaluation of thermal processing and properties of 422 martensitic stainless steel for replacement of 4140 steel in diesel engine pistons," *Materials & Design,* vol. 214, p. 110373, 2022.

[19] D. Pierce, R. Pillai, H. Wang, J. Poplawsky, J. Haynes, K. Sebeck, M. Tess, E. Gingrich and G. Muralidharan, "Overcoming the thermal conductivity versus oxidation resistance barrier in high-temperature steels," *Communications Materials,* vol. 6, p. 262, 2025.

[20] R. Pillai, J. A. Haynes, T. Lowe and D. Pierce, "Impact of hydrogen combustion on the oxidation-induced degradation of heavy-duty diesel engine piston materials," in *Association for Materials Protection and Performance*, 2025.

[21] E. Gingrich, M. Tess, V. Korivi and J. Ghandhi, "High-output diesel engine heat transfer: Part 1-comparison between piston heat flux and global energy balance," *International Journal of Engine Research,* vol. 23, pp. 1417-1431, 2022.

[22] NATO, *GUIDE SPECIFICATIONS (MINIMUM QUALITY STANDARDS) FOR AVIATION TURBINE FUELS (F 24, F 27, F 34, F 35, F 37, F 40 AND F 44) - AFLP-3747 EDITION C,* 2017.

[23] Y. Wang, M. Lance, J. Hayes, Z. Feng, D. Pierce, K. Sebeck, M. Tess and E. Gingrich, "Rotary inertia friction welding of dissimilar High-strength 422 martensitic stainless steel and 4140 low alloy steel for heavy-duty engine piston fabrication," *Welding Journal,* vol. 104, no. 3, 2024.

[24] Y. Wang, K. Sebeck, E. Gingrich, M. Tess, J. Haynes, G. Muralidharan, K. Will and D. Pierce, "Effect of post-weld heat treatment on microstructure and mechanical properties of rotary inertia friction welded dissimilar 422-4140 martensitic steel piston joints," *Journal of Materials Research and Technology,* 2025.

[25] Y. Wang, K. Sebeck, M. Tess, E. Gingrich, Z. Feng, J. Haynes, M. Lance, G. Muralidharan, R. Marchel, T. Kirste and D. Pierce, "Interfacial microstructure and mechanical properties of rotary inertia friction welded dissimilar 422 martensitic stainless steel to 4140 low alloy steel joints," *Materials Science and Engineering: A,* vol. 885, p. 145607, 2023.

[26] M. J. Tess, V. Korivi, E. M. Gingrich and P. Schihl, Influence of spray and combustion processes on piston temperatures and engine heat transfer in a high-output diesel engine, vol. 24, International Journal of Engine Research, 2023, pp. 2260-2278.

[27] E. Gingrich, M. Tess, V. Korivi, P. Schihl, J. Saputo, G. M. Smith, S. Sampath and J. Ghandhi, "The impact of piston thermal barrier coating roughness on high-load diesel operation," *International Journal of Engine Research,* vol. 22, pp. 1239-1254, 2021.

[28] K. Hart, M. Azevedo, J. Rebello and C. Ribeiro, "Bushingless Piston and Connecting Rod Assembly and Method of Manufacture". US Patent 6557457, 6 May 2003.

[29] M. Tess, "Initial Evaluation of a 422 Stainless Steel Piston in a Single-Cylinder Diesel Engine (Presentation Only)," in *SAE WCX*, 2025.

[30] S. Haugland, "3D mechanical and thermal analysis of an Aluminium piston for a high-speed Diesel laboratory engine," 2018.

[31] V. Lepingle, G. Louis, D. Allue and Lefebvre, "Steam oxidation resistance of new 12%Cr steels: Comparison with some other ferritic steels," *Corrosion science,* vol. 50, no. 4, pp. 1011-1019, 2008.

[32] Pint, "Addressing the Role of Water Vapor on Long-Term Stainless Steel Oxidation Behavior," *Oxidation of Metals,* vol. 95, pp. 335-357, 2021.

6. CONTACT INFORMATION

Eric M Gingrich, PhD

Specialist Research Engineer

Propulsion Branch
U.S. Army DEVCOM
Ground Vehicle Systems Center (GVSC)

6501 E. 11 Mile Road, MS 121

Warren, MI 48397
eric.m.gingrich.civ@army.mil
571-588-6860

7. ACKNOWLEDGMENT

The authors thank Mr. Steven Stoll for his technical support in the collection of the engine data, and the others in GVSC's propulsion laboratory for their contributions throughout the duration of this project. This work was in part funded by Army In-House Laboratory Independent Research (ILIR) basic research funds.

8. ACRONYMS

°aTDC	degrees after top dead center
BDC	bottom dead center
CA50	50% cumulative apparent heat release
CFD	computational fluid dynamics
HD	heavy-duty
IMT	intake manifold temperature
ITEg	gross indicated thermal efficiency
MAS	microalloyed steel
MnP	manganese phosphate
PCN	piston cooling nozzle
SOI	start of injection
TC	thermocouple

9. APPENDIX

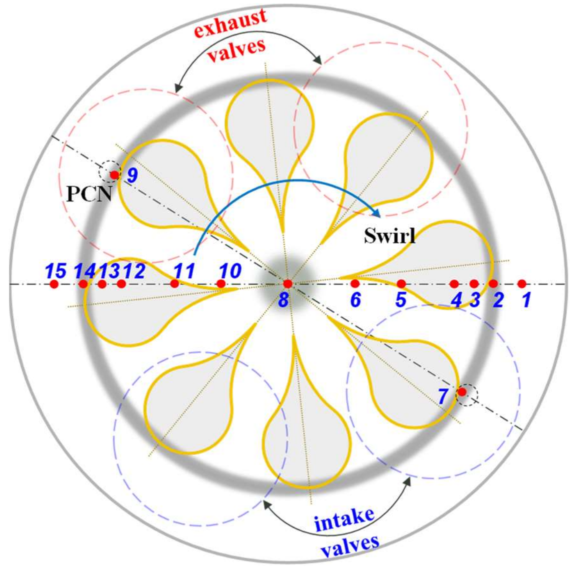

Figure A.1: Top view of piston showing fuel spray targeting (adapted from [26])

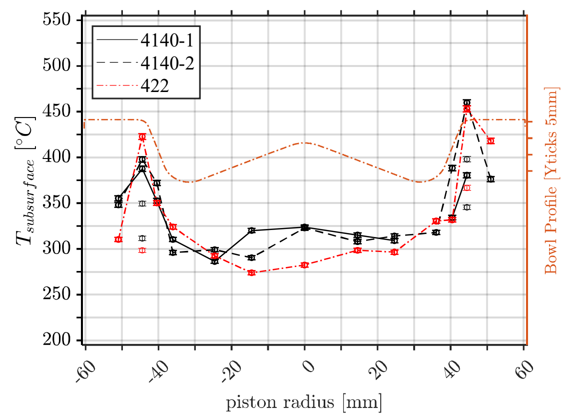

Figure A.2: Operating condition 2, CA50=2°aTDC, subsurface piston temperature versus piston radial location for 4140-1, 4140-2, and 422. The piston bowl profile is outlined by the dash-dot orange line (right y-axis).

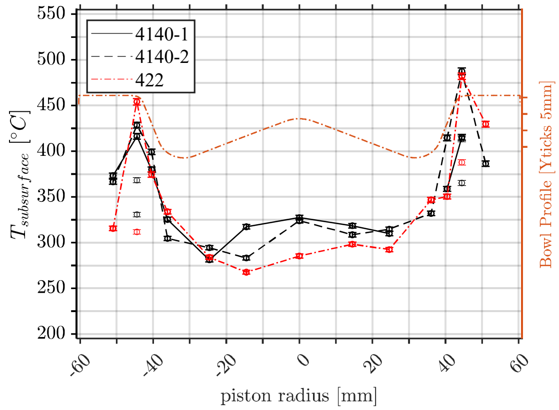

Figure A.3: Operating condition 4, CA50=13°aTDC, subsurface piston temperature versus piston radial location for 4140-1, 4140-2, and 422. The piston bowl profile is outlined by the dash-dot orange line (right y-axis).

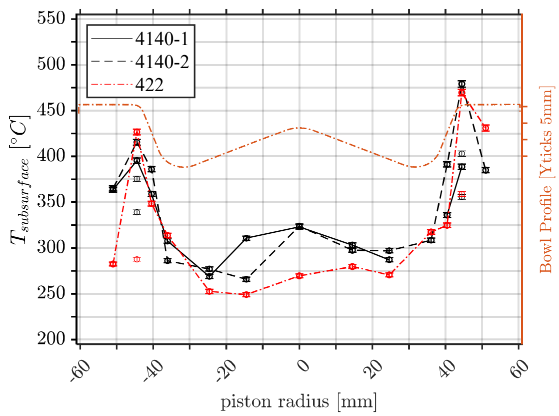

Figure A.4: Operating condition 5, CA50=17°aTDC, subsurface piston temperature versus piston radial location for 4140-1, 4140-2, and 422. The piston bowl profile is outlined by the dash-dot orange line (right y-axis).

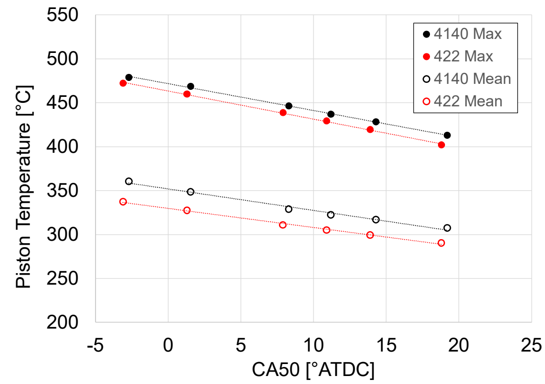

Figure A.5 Operating condition 3 subsurface piston temperature versus CA50 for 4140-2 and 422. The maximum temperature location (TC2) is shown with filled circles, and the average temperature is shown with open circles.

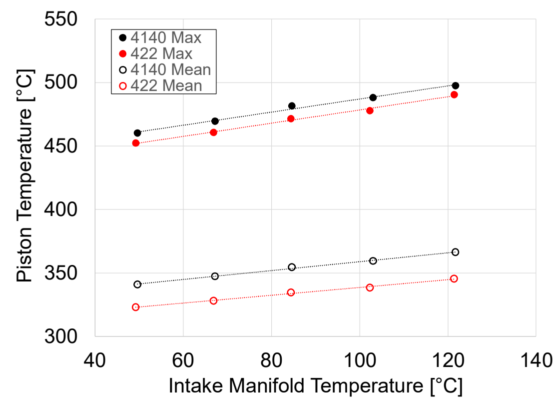

Figure A.6: Operating conditions 3, CA50=-3.5°aTDC, subsurface piston temperature versus intake manifold temperature for 4140-2 and 422. The maximum temperature location (TC2) is shown with filled circles, and the average temperature is shown with open circles.

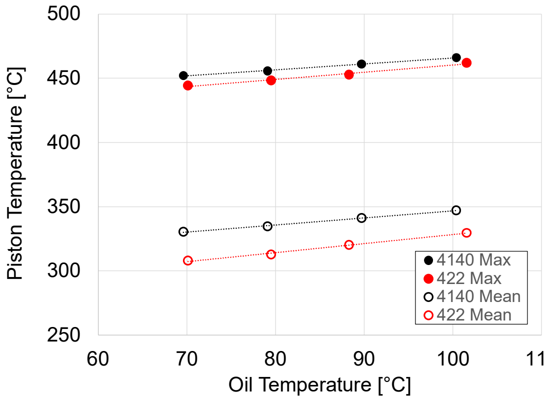

Figure A.7: Operating conditions 3, CA50=2°aTDC, subsurface piston temperature versus oil temperature for 4140-2 and 422. The maximum temperature location (TC2) is shown with filled circles, and the average temperature is shown with open circles.

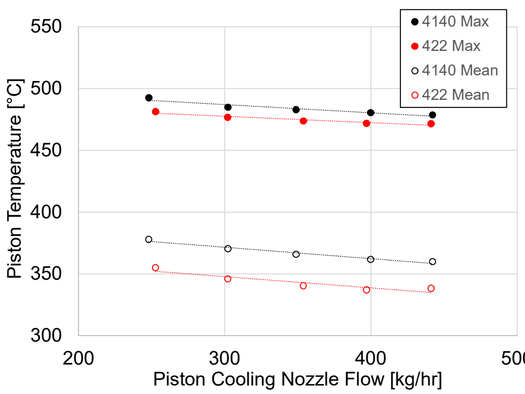

Figure A.8: Operating conditions 3, CA50=-3°aTDC, subsurface piston temperature versus PCN flow for 4140-2 and 422. The maximum temperature location (TC2) is shown with filled circles, and the average temperature is shown with open circles.

Table A.1. Detailed chemical composition in wt%. 4140 from [17] and 422 from [18]

Element	4140	422
Ni	0.21	0.79
Mn	0.88	0.78
C	0.41	0.23
Cr	0.99	12.09
Si	0.26	0.36
V	0.001	0.22
Mo	0.21	1.08
Cu	0.17	0.08
W	-	0.96
Al	0.026	0.001
N	-	0.048
S	0.012	0.006
P	0.009	0.019
O	-	0.006
Ti	-	-
Co	-	0.02
Nb		0.026
B	3.00E-04	-
Fe	Bal.	Bal.